7th World Congress on Structural and Multidisciplinary Optimization
COEX Seoul, 21 May – 25 May 2007, Korea

AERODYNAMIC SHAPE OPTIMIZATION USING OVERSET MESH TECHNIQUE FOR MULTIPLE BODY AIRCRAFT GEOMETRIES

Byung Joon Lee, Jin Woo Yim, Sung-Hwan Yoon [1], Chongam Kim[2]

[1]Ph.D. Student, [2]Professor, E-mail : chongam@snu.ac.kr
School of Mechanical & Aerospace Engineering, Seoul National Unversity, Seoul, Korea.

1. Abstract

A new design approach for a delicate treatment of complex geometries such as wing/body configuration is arranged using overset mesh technique under large scale computing environment. For the in-depth study of the flow physics and highly accurate design, several special overlapped structured blocks such as collar grid, tip-cap grid, and etc. which are commonly used in refined drag prediction are adopted to consider the applicability of the design code to practical problems. Various pre- and post-processing techniques for overset flow analysis and sensitivity analysis are devised or implemented to adapt overset mesh technique to the design optimization problem based on Gradient Based Optimization Method (GBOM). In the pre-processing, the convergence characteristics of the flow solver and sensitivity analysis are improved by overlap optimization method. Moreover, a new post-processing method, Spline-Boundary Intersecting Grid (S-BIG) scheme, is proposed by considering the ratio of cell area for more refined prediction of aerodynamic coefficients and convenient evaluation of sensitivities under parallel computing environment. For the sensitivity analysis, adjoint formulations for overset boundary conditions are implemented into the fully hand-differentiated sensitivity analysis code. A smooth geometric modification on the overlapped surface boundaries and evaluation of grid sensitivities can be performed by mapping from planform coordinate to the surface meshes with Hicks-Henne function. Careful design works for the drag minimization problem of a transonic wing and a wing/body configuration are performed using the newly-developed and -applied overset mesh techniques. And the design results from conventional design problem demonstrate the capability of the present design approach successfully.

2. Keywords: Discrete Adjoint Variable Method, Overset Approach, Optimal Shape Design, S-BIG (Spline-Boundary Intersecting Grid), Complex Geomtry

3. Introduction

In aerodynamic shape optimization (ASO) for aircraft, GBOM (Gradient Based Optimization Method) is generally used because it is very efficient method to find optimum shape and it can be easily applied to the MDO frameworks. Typical GBOM consists of four elements: Flow solver, sensitivity analysis code, grid generator (or grid modifier), and optimization algorithm. Most of all the components, an accurate and efficient flow solver is overriding concern to evaluate the pressure distribution and aerodynamic loads such as lift, drag and pitching moment that compose the objective functions to be optimized. The recent trends in the development of flow solver are 'large scale' and 'complex geometry'. As the computational environment rapidly develops, the interests of CFD are focused on large-scale computations over complex geometries.[1, 2] Keeping pace with these trends, various grid techniques are used in the flow analyses and design optimization problems over complex geometries.

The design problem of multiple body aircraft geometries have been a matter of concern since late 1990s. Design method using multi-block system doesn't require any additional new techniques as compared with single block problems. Therefore as a straightforward extension of single block case, multi block system is easily applied to design of wing/body configurations and full body supersonic aircraft by numerous researchers.[3-5] Multi-block grid technique can secure a good grid quality. However, in case of moving grid or deforming grid applications, severe grid changes or even the grid topology changes are inevitable and these works cannot be performed fully automatically under multi-block environment. On the other hand, in case of unstructured grid system, the automatic mesh deformation can be easy work. In this reason, unstructured discrete adjoint variable codes are developed by, Nielsen(1998)[6], Kim(2000)[7] Jameson(2001)[8] et al. Nevertheless, compared with the structured grid, far more grid points are needed to analyze the flow in keeping the same resolution of solution. And additionally, it requires much more memory and computational time cost than the structured grid does even with the same number of grid points.

In view of these issues, the overset grid technique has several benefits to be applied to the large scale flow analysis and design optimization problems. At first, the grid topology is relatively simple to represent the deforming grid. Secondly, the movement of the grids, the change of the part position, and the exchange of parts are easily implemented. On the third,

high-resolved flow solutions can be obtained through a relatively small number of grid points. Finally, the fully automatic grid-generation is possible because of the simple grid topology. These characteristics of overset mesh technique can derive the design optimization to the final goal, 'fully automatic aerodynamic design from CAD models'. Development of adjoint variable codes based on overset mesh system is performed by only a few researchers. Multi-element airfoil with hand-differentiation of two-equation turbulence model is performed by Kim et al. [9] In case of three-dimensional problem a simple turbine vane design is carried out by Liau et al. They applied continuous adjoint approach for Euler-equations using implicit hole-cutting method to the design work.[10]

In the present paper, we applied several major pre- and post-processing methods for overset mesh system to aerodynamic shape design based on discrete adjoint approach. These techniques are newly devised or adapted for sensitivity analysis and design problem. Thus, Spline-Boundary Interpolation Grid(S-BIG) scheme for easy calculation of cell differentiation, and the overlap optimization[12] for high quality flow analysis results and good convergence characteristics of adjoint variable code are resolved in the design optimization tools for complex geometries. Exploiting these techniques a drag minimization problem for DLR-F4 wing/body configurations in the overset grid system composed of typical 4 component blocks and 3 box blocks are carried out. [13]

4. Numerical Approach

4.1. Overlap Optimization for Overset Adjoint Code

As mentioned above main focus of the present work is on the application of adjoint approach in discrete manner to the complex overset mesh system. Recently there are many progresses in flow analysis techniques for overset mesh system. The main issues of the overset flow analysis codes are focused upon the preprocessors such as PEGSUS[12], DCF3D[14], Beggar[15], Overture[16] and etc. These are high quality overset preprocessors. Especially, PEGASUS is one of the most efficient and robust code and a tremendous number of applications, i.e., flow analyses of very complex geometries as like full body aircraft, space craft, turbine blade, and so on, are carried out using this preprocessing code in NASA. In these applications, the number of the overlapped blocks is too many and the block connectivity of grid systems is inevitably so complicated to resolve the complicated flow phenomena with refined definition of analysis. As a result, an automatic finding process for hole-searching and construction of block connectivity are applied to the latest version. This technique is named by overlap optimization. This method can improve the convergence characteristics of overset analysis code by considering the ratio of cell volume or cell aspect ratio of donor and fringe cells. In addition, it can diminish the oscillation of the overset solution by minimizing overlapped different computation region in one physical space. The present sensitivity analysis code in adjoint approach is definitely affected by the oscillation of the overset solution, too.

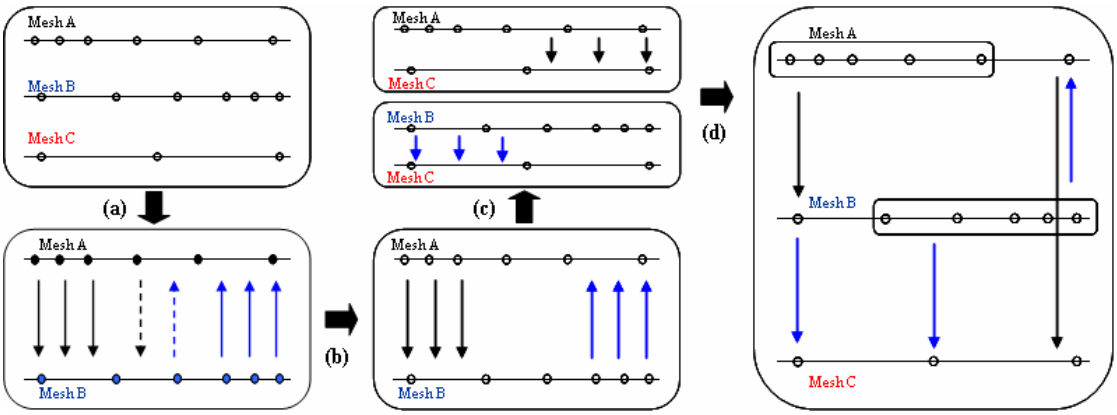

Fig. 1. Procedure of Overlap Optimization[12]

The basic concept of overlap optimization is presented in Fig. 1. In order to construct the block connectivity between simple three 1-dimensional overlapped blocks having different grid distribution as shown in Fig. 1-(a), the flow variables in the overlapped region are calculated with flux function and those of all the coarser cells are updated by interpolation. For accurate and robust interpolation, the donor cells for each fringe cell are selected by considering the cell-difference parameter (CDP). The CDP is defined as:

$$CDP = \sum_{j=1}^{3} \frac{(X_j)_{DB} V_B - (X_j)_{DI} V_I}{(X_j)_{DB} V_B} \tag{1}$$

where $(X_j)_{DB}$ is the maximum of the j[th] component of the four diagonals of the boundary cell (one of the candidates of the donor cell), $(X_j)_{DI}$ is the maximum of the j[th] component of the four diagonals of the interpolation cell (fringe cell), V_B is

the volume of the minimum Cartesian cell encompassing the boundary cell, and V_I is the volume of the minimum Cartesian cell encompassing the interpolated cell. CDP will vary from 0 (the best) to very large values. [12] And equation (1) comprises that this parameter can represent the difference of cell aspect ratio and cell volume simultaneously. In case there is fringe to fringe interpolation as shown in Fig. 1–(b) and (c), the region is determined as computational domain by removing the relation of interpolation. Finally, the left region of block A and right region of block B will be the computational domain and other regions are updated by interpolation with the block connectivity in Fig. 1-(d). For more details about overlap optimization process, refer to Ref.[12].

Figure 2 shows the comparison of computational domain of the manually assigned case and overlap optimized case for fuselage block of DLR-F4 wing/body configuration. The overlapped computational regions where two or more solutions coexist in the same physical space are minimized. The flow analysis results in Fig. 3 show the overlap optimization can secure the convergence characteristics of the flow solver and guarantee more refined solutions. The convergence characteristics of adjoint code cannot be secured without the overlap optimization, either. Because the major premise of the adjoint approach is that the flow solutions should be well converged and the residual on each cell be almost zero. The convergence characteristics for adjoint code with and without overlap optimization for ONERA-M6 wing with 2-blocks overset system are compared in Fig. 4(Left). This figure shows that manual hole-cutting and donor finding routines cannot secure stable convergence of the adjoint variable code. And the overset adjoint code is tested in 7 block system of DLR-F4 wing/body configuration to validate the sensitivity code in a complicated overset mesh system. The residual history shows that the adjoint code is converged very well on all the blocks in Fig. 4(Right).

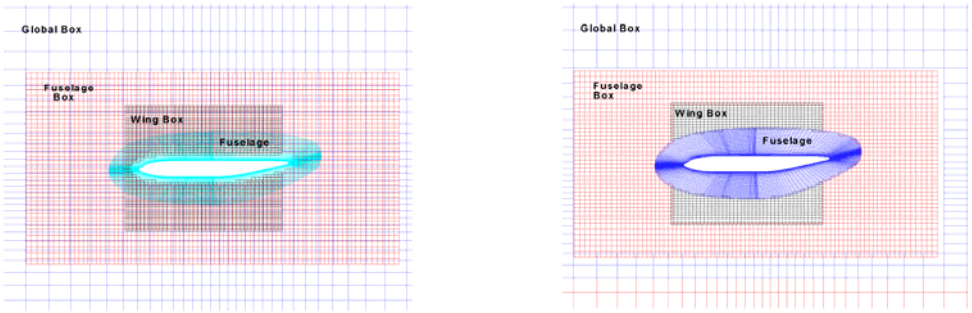

Fig. 2. Comparison of Computational Domain
[Manually Assigned Case(Left) and Overlap Optimized Case(Right)]

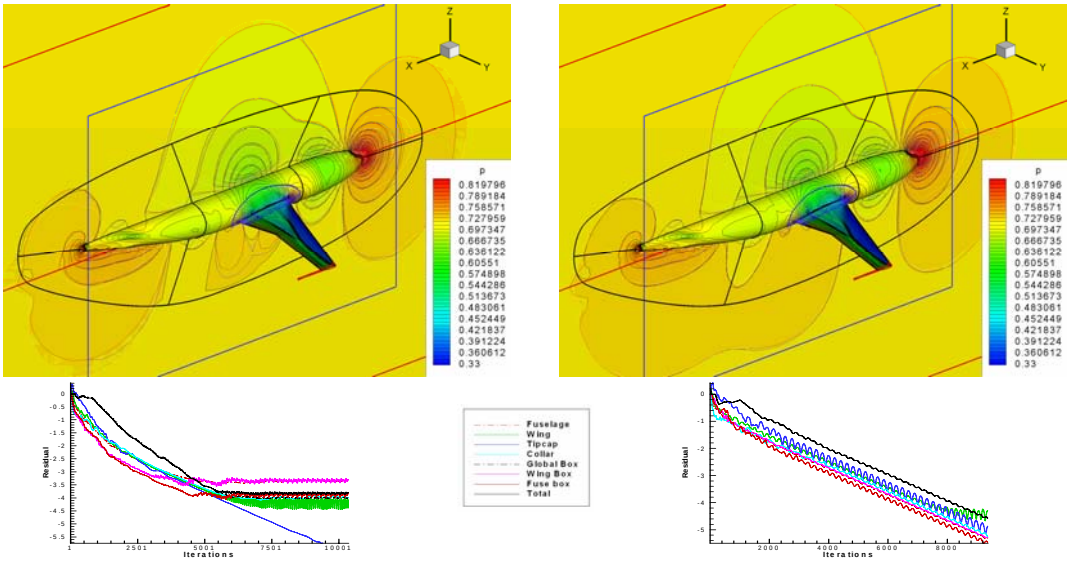

Fig. 3. Comparison of Flow Analysis Results without(Left) and with(Right) Overlap Optimization

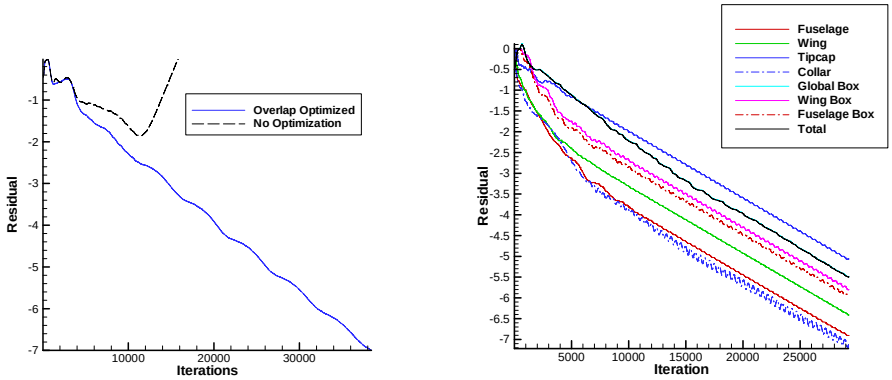

Fig. 4. Residual History of Overlap Optimized Overset Adjoint Code
[Left: 2 Block Overset Mesh system(ONERA-M6), Right: 7 Block Overset Mesh System(DLR-F4)]

4.2. Spline-Boundary Intersecting Grid (S-BIG) Scheme

4.2.1. Main Cell Reformation

In case of post processor for overset flow analysis, Zipper grid scheme[17] is widely used in calculation of aerodynamic coefficients. Zipper grid is a kind of grid reconstruction method. This method consists of blanking process of overlapped region and reconstruction process with an unstructured surface grid set. The flow variables on the zipper grid are interpolated from donor cells of computational overlapped blocks around the same physical point. However, the flux differential terms from arbitrary number of donor cells make it difficult to apply this method to adjoint variable code. In the present work, a newly devised Spline-Boundary Intersecting Grid (S-BIG) scheme is applied to the post processing routine and sensitivity analysis to make the differentiation process easy. The objective of S-BIG is preparation of evaluating routines for aerodynamic coefficients that require no interpolation process from donor cells. Assuming that Zipper grid scheme is reconstruction of grids on the level of a block, S-BIG is reconstitution of grids on the level of a cell. Thus arbitrary number of information transferal between blocks, which makes difficulties in differentiation of objective functions, is not necessary because this method does not requires except the boundary information to reform surface grid cell. S-BIG scheme is composed by 4 stages. On the first stage, boundaries of the overlapped surface are determined by user. In case of the interface between fuselage and collar block, the outer boundary of the collar grid is chosen as shown in Fig. 5. The interfaces on wing surface such as collar-wing, wing-tipcap boundaries can be specified by a constant line(y=constant). And the determined boundaries can be parameterized by B-Spline function. The next process is dividing the surface grid points into inner and outer vertices based on the Spline boundary. The outer vertices are set as normal vertices (NBLAK=1) and the inner as blanked vertices (NBLANK=0) as like hole cutting process as shown in Fig. 6-(a). Then there are 16 cases for inner and outer vertex distribution on a surface cell as shown in Fig. 6-(b). The surface cells are classified by 3 kinds of cells as like conservative Chimera scheme. 18 They are named by normal cell, cut cell, blanked cell and this classification is given in Fig.6.

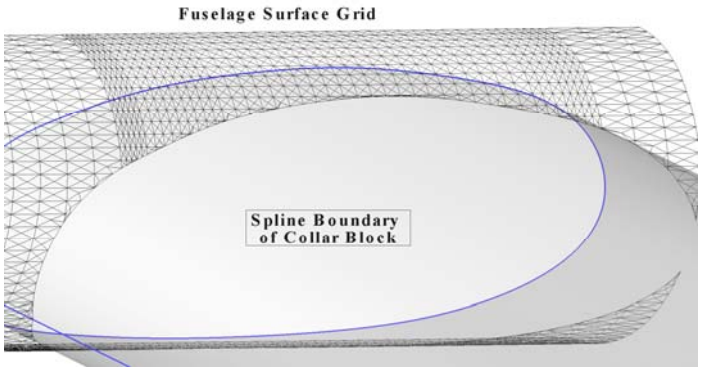

Fig. 5. Spline boundary of collar block at the interface with fuselage surface

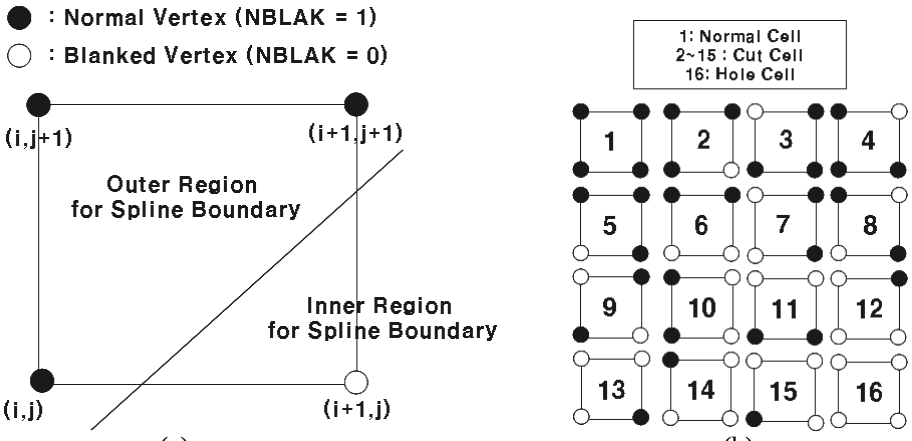

(a) (b)

Fig. 6. (a) Blanking process by spline boundary (b) Classification of blanked surface cells

For the structured grid system, a surface cell is typically a square which has 4 vertices. On the 3rd stage, the intersection between Spline boundary and 4 edges of each square surface cell is evaluated. The role of spline boundary information is to cut out blanked area of overlap cell for the cell reconstruction process as represented in Fig. 7-(a). For this process, all the square surface cells are expressed by 8 vertices and 8 triangles for cell deformation by intersection in the Fig. 7-(b). Two vertices are allocated on each vertex of square surface cell and a center point can be evaluated on the averaged point of 4 vertices of the square. Then the eight triangles A-G are generated on the cell. As a matter of course, the area of B, D, F, H is zero. These vertices and triangles are adopted to represent the cell area any deformed surface cell by intersection and to evaluate the cell area of the deformed cell. In Fig.7-(c), the vertices allocated on the blanked vertex are displaced to the intersection point with spline boundary. Finally, cut cell case 2 can be deformed as like Fig. 7-(d). This figure shows an example of case 2. And the other cases (3~15) can be expressed by adequate movement of blanked vertex to intersection point. This may be easily determined by users on a case-by-case basis.

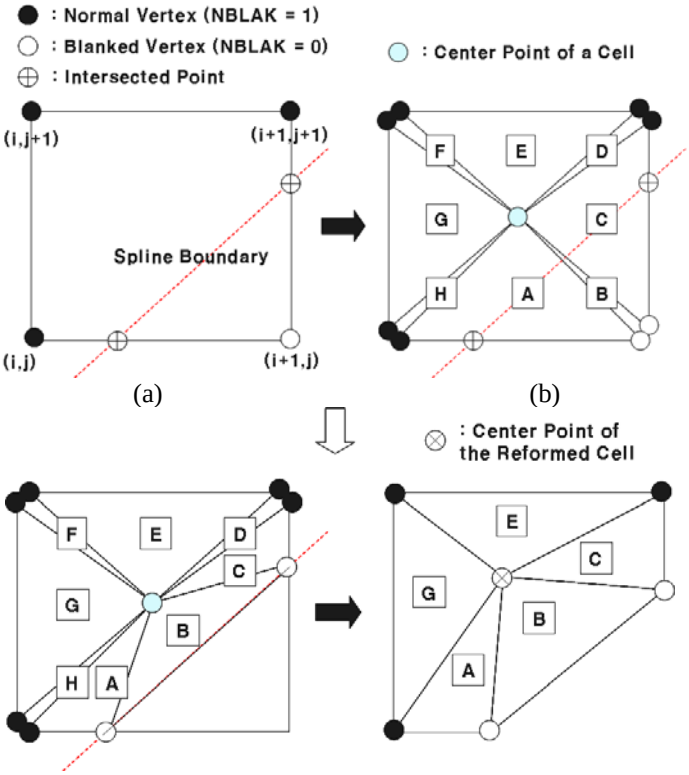

(a) (b)

(c) (d)

Fig. 7. Reconstruction of cut-clls (a) Initial blanked cut cell (b) 8 vertex & 8 triangle form of a surface cell (c) Displacement of blanked vertices (d) Calculation of cell area of reformed cut cell

2.2.2. Addition of Extra Triangles for Error Correction

The deformed cut cell on the curved boundary as like collar-fuselage interface may deteriorate the accuracy of the predicted aerodynamic coefficients because the curved boundary line case as shown in Fig. 8-(a) is not considered in the main cell deformation process. Therefore the area of extra-triangles composed by 2 intersection points and boundary points included inner region the cell should be incorporated as shown in Fig. 8-(b). The area of each triangle can be easily evaluated using the vertex point information. And the area of surface cut-cells can be finally acquired by subtraction or summation of reformed main cell area and extra-triangle area.

2.2.3. Integration of Aerodynamic Coefficients

On the last sequence, the cell area is calculated by the summation of areas of 8 triangles on each surface cell except blanked cell. In case of hole-cell, the surface cell area is set to 0. And aerodynamic coefficients are integrated using the evaluated surface cell-area. Surface grid set of DLR-F4 reconstructed by S-BIG scheme is presented in Fig. 9.

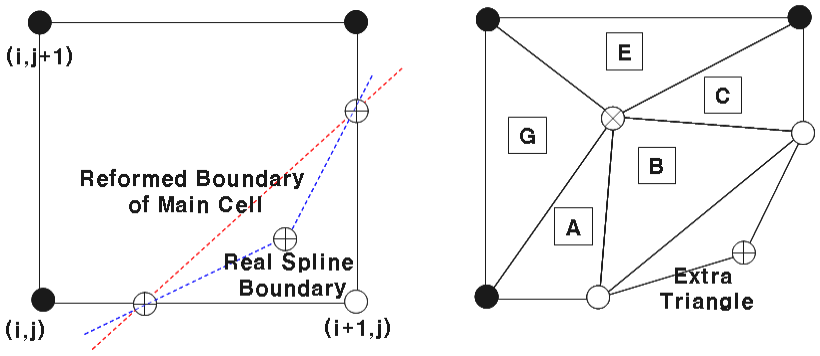

(a) (b)

Fig. 8. Incorporation of Extra-Triangle in Cut-Cells
[(a) Concave type Spline-boundary (b) Addition of Extra-Triangle]

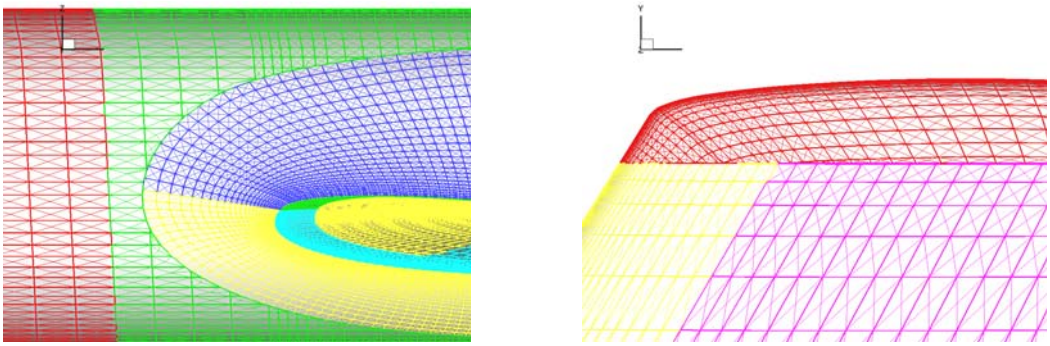

(a) Interface at Fuselage-Collar Blocks (b) Interface at Wing-Tipcap Blocks

Fig. 9. Reconstructed surface grid on DLR-F4 W/B configuration

4.3. Sensitivity Analysis for Overset Boundary

The formation of discrete adjoint variable method with overset boundary formulations are presented in this chapter. The brief explanation of discrete adjoint variable method is as follows.

The discrete residual of the steady-state flow equations can be written as

$$\{R\} = \{R(Q, X, D)\} = \{0\} \tag{2}$$

where Q is the flow variable vector, X is the computational grid position and D is the vector of design variables. Similarly, the vector of the aerodynamic objective function F to be either minimized or maximized is also dependent on Q, X and D as

$$\{F\} = \{F(Q, X, D)\} = \{0\} \tag{3}$$

The sensitivity derivatives of the aerodynamic function are calculated by directly differentiating Eqs. (2) and (3) with respect to D as

$$\left\{\frac{dR}{dD}\right\} = \left[\frac{\partial R}{\partial Q}\right]\left\{\frac{dQ}{dD}\right\} + \left[\frac{\partial R}{\partial X}\right]\left\{\frac{dX}{dD}\right\} + \left\{\frac{\partial R}{\partial D}\right\} = \{0\} \tag{4}$$

$$\left\{\frac{dF}{dD}\right\}=\left\{\frac{\partial F}{\partial Q}\right\}^T\left\{\frac{dQ}{dD}\right\}+\left\{\frac{\partial F}{\partial X}\right\}^T\left\{\frac{dX}{dD}\right\}+\left\{\frac{\partial F}{\partial D}\right\} \tag{5}$$

Efficient evaluation of {dQ/dD} from Eq. (4) is required in problems involving many design variables. In adjoint variable methods, the sensitivity derivatives of the aerodynamic function are obtained by combining Eq. (4) with Eq. (5) as

$$\left\{\frac{dF}{dD}\right\}=\left\{\frac{\partial F}{\partial Q}\right\}^T\left\{\frac{dQ}{dD}\right\}+\left\{\frac{\partial F}{\partial X}\right\}^T\left\{\frac{dX}{dD}\right\}+\left\{\frac{\partial F}{\partial D}\right\}+\Lambda^T\left(\left[\frac{\partial R}{\partial Q}\right]\left\{\frac{dQ}{dD}\right\}+\left[\frac{\partial R}{\partial X}\right]\left\{\frac{dX}{dD}\right\}+\left\{\frac{\partial R}{\partial D}\right\}\right) \tag{6}$$

where Λ represents the 7-element adjoint vector. Rearranging Eq. (6) yields the following equation.

$$\left\{\frac{dF}{dD}\right\}=\left\{\frac{\partial F}{\partial X}\right\}^T\left\{\frac{dX}{dD}\right\}+\left\{\frac{\partial F}{\partial D}\right\}+\Lambda^T\left(\left[\frac{\partial R}{\partial X}\right]\left\{\frac{dX}{dD}\right\}+\left\{\frac{\partial R}{\partial D}\right\}\right)+\left(\left\{\frac{\partial F}{\partial Q}\right\}^T+\Lambda^T\left[\frac{\partial R}{\partial Q}\right]\right)\left\{\frac{dQ}{dD}\right\} \tag{7}$$

Without the necessity of evaluating the vector {dQ/dD}, the sensitivity derivatives of the aerodynamic function can be calculated as

$$\left\{\frac{dF}{dD}\right\}=\left\{\frac{\partial F}{\partial X}\right\}^T\left\{\frac{dX}{dD}\right\}+\left\{\frac{\partial F}{\partial D}\right\}+\Lambda^T\left(\left[\frac{\partial R}{\partial X}\right]\left\{\frac{dX}{dD}\right\}+\left\{\frac{\partial R}{\partial D}\right\}\right) \tag{8}$$

if and only if the adjoint vector Λ satisfies the following adjoint equation.

$$\left[\frac{\partial R}{\partial Q}\right]^T\Lambda+\left\{\frac{\partial F}{\partial Q}\right\}^T=\{0\}^T \tag{9}$$

The solution vector Λ is obtained by solving the Euler implicit method of Eq. (9) time-iteratively as

$$\left(\frac{I}{J\Delta t}+\left[\frac{\partial R}{\partial Q}\right]_{VL}^T\right)\Delta\Lambda=-\left[\frac{\partial R}{\partial Q}\right]^T\Lambda^m-\left\{\frac{\partial F}{\partial Q}\right\}^T \tag{10}$$

$$\Lambda^{m+1}=\Lambda^m+\Delta\Lambda \quad (\text{update vector}\,\Lambda\,\text{of}\,(m+1)^{\text{th}}\,\text{step})$$

where I is identity matrix, and J represents Jacobian matrix, and the subscript VL means the Van-Leer flux Jacobian. The adjoint equation (10) is solved by a time integration scheme with the boundary conditions of Eq. (11), (12).

$$\left[\frac{\partial R}{\partial Q}\right]^T\Lambda+\left[\frac{\partial R_B}{\partial Q}\right]^T\Lambda_B+\left\{\frac{\partial F}{\partial Q}\right\}^T=\{0\}^T \tag{11}$$

$$\left[\frac{\partial R}{\partial Q_B}\right]^T\Lambda+\left[\frac{\partial R_B}{\partial Q_B}\right]^T\Lambda_B+\left\{\frac{\partial F}{\partial Q}\right\}^T=\{0\}^T \tag{12}$$

where subscript B represents boundary cell. In Eq.(12), adjoint variable Λ_B of boundary cell is updated by inner cell-values of n th time step. And the variables of the next time step (n+1) are evaluated by Eq.(11) using the boundary values from (12). Overset boundary conditions can be derived by a similar way to the conventional adjoint boundary conditions except the number of equations as like Eq. (13)-(16).

$$\left[\frac{\partial R^M}{\partial Q^M}\right]^T\Lambda^M+\left[\frac{\partial R_F^S}{\partial Q^M}\right]^T\Lambda_F^S+\left\{\frac{\partial F^M}{\partial Q^M}\right\}^T=\{0\}^T, \tag{13}$$

$$\left[\frac{\partial R^S}{\partial Q^S}\right]^T\Lambda^S+\left[\frac{\partial R_F^M}{\partial Q^S}\right]^T\Lambda_F^M+\left\{\frac{\partial F^S}{\partial Q^S}\right\}^T=\{0\}^T, \tag{14}$$

$$\left[\frac{\partial R^M}{\partial Q_F^M}\right]^T\Lambda^M+\left[\frac{\partial R_F^M}{\partial Q_F^M}\right]^T\Lambda_F^M+\left\{\frac{\partial F^M}{\partial Q_F^M}\right\}^T=\{0\}^T, \tag{15}$$

$$\left[\frac{\partial R^S}{\partial Q_F^S}\right]^T\Lambda^S+\left[\frac{\partial R_F^S}{\partial Q_F^S}\right]^T\Lambda_F^S+\left\{\frac{\partial F^S}{\partial Q_F^S}\right\}^T=\{0\}^T, \tag{16}$$

where the subscript F represent fringe cells and the superscript M and S represent the main grid and sub-grid domain respectively. Through these 4 system equations, each overset boundary values can be updated to inner adjoint variables of the next time step. Inner values of sub-grid domain are evaluated by Eq. (15), (14) orderly. And for the main-grid domain calculations are carried out from (16) to (13).

5. Observations

5.1. Test Cases & Grid Systems

5.1.1. Overset Grid System for Design Problem

For the design optimization, two test geometries are adopted. 2 block system of ONERA-M6 wing is used in the validation of the overset solver and the adjoint code. The mesh system consists of wing block $(143\times39\times33)$ and global box block $(63\times27\times63)$. The wing block is constructed by O-O type grid and the box grid is a Cartesian grid as shown in Fig. 10-(a). The total number of mesh points is about 300 thousands pts.

And DLR-F4 wing/body configuration is applied for more practical complicated problem. Large scale computations over wing/body configurations are actively performed in flow analysis and aerodynamic shape optimization field. In the 1st Drag Prediction Workshop (DPWI), the provided test geometry of drag prediction is DLR-F4, which consists of wing and fuselage. [2, 13] Figure 10-(b) show the overall mesh system of 7 blocks over DLR-F4. Those 7 blocks are global box $(77\times38\times72)$, fuselage box $(84\times26\times45)$, wing box $(44\times37\times54)$, fuselage block $(190\times41\times30$: O-O type), collar block $(146\times26\times26$: O-H type), wing block $(143\times43\times34$: O-H type), and tipcap block $(103\times43\times42$: C-type). All the box blocks are simple Cartesian grids. The total number of mesh points (7 blocks) is about 1.22 million. To guarantee a good mesh quality, collar block is positioned at the interface of wing and fuselage and tipcap block on the wing tip. The fuselage block is made up of 1 block using untrimmed approach. The overset mesh systems used in the present work are shown in Fig. 10-(a) and (b).

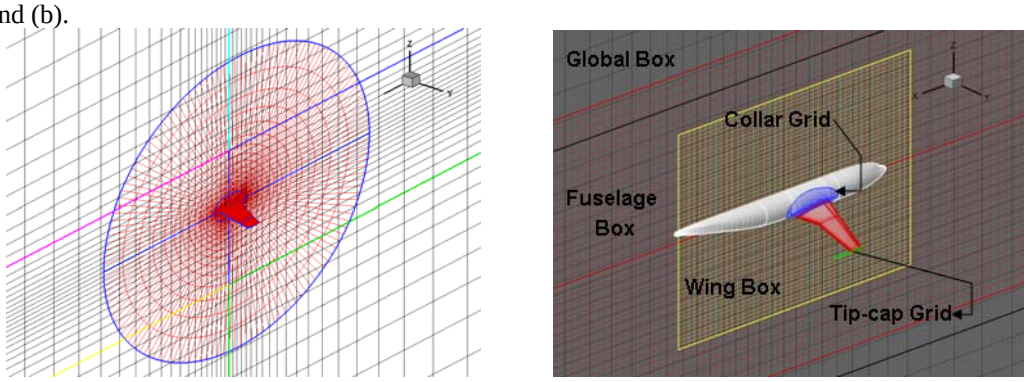

(a) ONERA-M6 (2Blocks) (b) DLR-F4 (7 Blocks)

Fig. 10. Overset Mesh System for the Test Cases

5.1.2. Flow Conditions & Numerical Techniques

The flow conditions for ONERA-M6 wing are that the free stream Mach number is 0.84 and the angle of attack is 3.06 degree, which is a well-known case where the lamda shock is observed on the wing surface. And those of DLR-F4 are that free stream Mach number is 0.75 and angle of attack is 0.0 degree. Those flow conditions are a validation case of DPWI.

The governing equations are the three-dimensional compressible Euler equations. The governing equations are transformed in generalized coordinates and are solved with a finite-volume method. For the calculation of residual, convective terms are upwind-differenced based on RoeM scheme by Kim et al.[19] A MUSCL (Monotone Upstream Centered Scheme for Conservation Laws) approach using a third order interpolation is used to obtain a higher order of spatial accuracy in all calculations. For temporal integration, Yoon's LU-SGS scheme is applied.

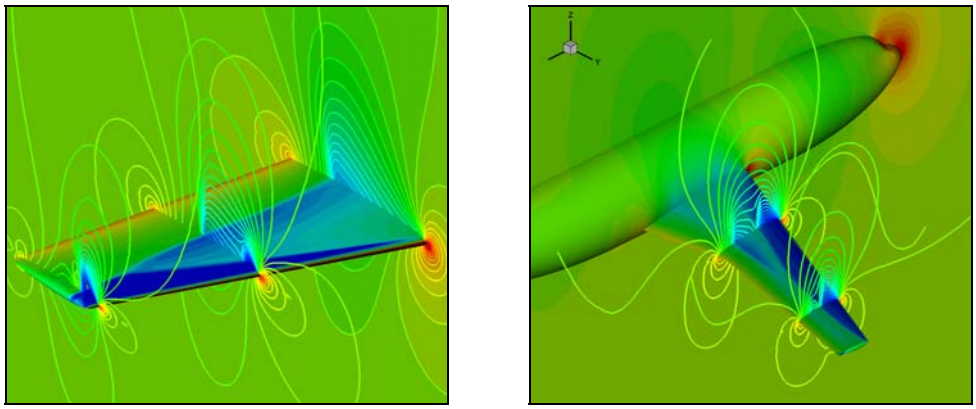

(a) ONERA-M6 (b) DLR-F4

Fig. 11. Flow Analysis Results (Pressure Contours)

The flow analysis results of the two tests cases are presented in Fig. 11. Those show that the block to block interpolation is carried out very well. In both of the cases, a complex shock configuration is observed on the upper wing surface and drag minimization will be presented through weakening the shock-strength in the next chapter.

5.2. Sensitivity Analysis & Design Optimization

5.2.1. Validation of Sensitivity Analysis

The design variables used in the validation of overset adjoint code are 20 Hicks-Henne functions on each design section of ONERA-M6 wing. And 10 Hicks-Henne functions are imposed on upper and lower surface, respectively for a design section. The geometric modification is performed on 3 design sections at wing root, mid point, and wing tip. The deformation of other wing sections is evaluated by the linear-interpolation from the design sections. Totally, the number of the design variables used is 60. The gradient values of lift and drag coefficients for each design variable from adjoint approach are compared with the complex step derivatives (step size 10^{-8}) in Fig.12. [20] All the gradients agree very well with the complex step derivatives.

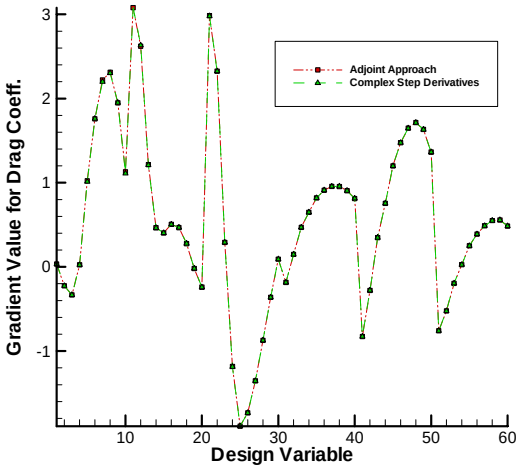

Fig. 12. Validation of Sensitivity Analysis

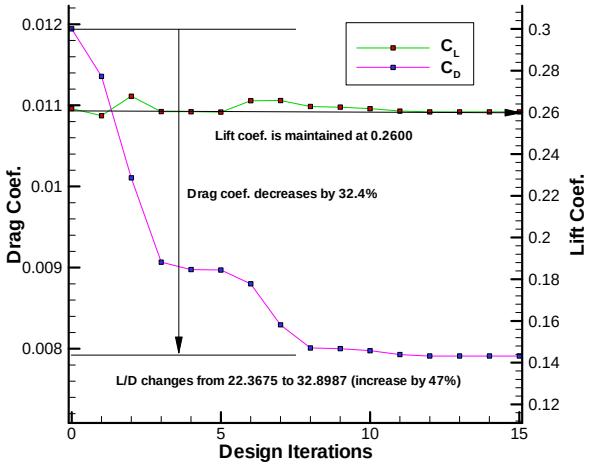

Fig. 13. Design History (ONERA-M6)

5.2.2. Drag Minimization of Transonic Aircraft Geometries

The presented overset design approach is applied to design optimization of a transonic wing and W/B configuration. Optimization is performed using the Broydon-Fletcher-Goldfarb-Shanno (BFGS) variable metric method which is a kind of non-constrained optimization technique and supported by the DOT (Design Optimization Tool) commercial software. For the first application of overset GBOM tool, a shock-free problem on a transonic wing, ONERA-M6, is performed by minimization of drag with maintaining a constant lift coefficient. This problem is very common problem for the performance test of GBOM tool. The number of design variables used in this problem is 60 which is same number to the validation case. The design problem is defined by Eq. (17). And as well known, the lift constraint is given by a form of penalty function as like Eq. (18) to prevent computational ineffectiveness of sensitivity analysis using adjoint approach. To guarantee the balanced variation of objective function and the penalty function, the weighting factor for the lift constraint is given by the ratio of the sensitivities of lift coefficient and drag coefficient for angle of attack.

$$Minimize: C_D$$

$$Subjected\ to: C_L \geq C_{L_0},\ C_{L_0} = (Lift\ Coefficient\ of\ Baseline\ Model) \tag{17}$$

$$(Objective\ Function) = C_D + Wt \times [0, C_{L_0} - C_L],\ Wt = \frac{\partial C_D}{\partial \alpha} \Big/ \frac{\partial C_L}{\partial \alpha} \tag{18}$$

After design process, the drag coefficient dramatically decreases as shown in Fig. 13. The design history shows the design process is converged well and the drag coefficient is changed from 0.0118 to 0.0079 (32% reduction) through 15 design iterations in maintaining lift coefficient at 0.2600. L/D is changed from 22.37 to 32.90 (47% increase). The pressure contours on the baseline ONERA-M6 wing and the designed wing are compared in Fig. 14. It can be observed that the Λ shock on the wing upper surface decreases considerably. The Cp curves and shapes of wing sections on the designed wing notify that the flow acceleration right after leading edge decreases owing to the deformation of wing nose. And it can be induced through the Cp curves that the effect of wave drag on the surface is considerably diminished. Through the shock free problem of ONEAR-M6 wing, the present design tool show its capability and applicability to the transonic aerodynamic design problems.

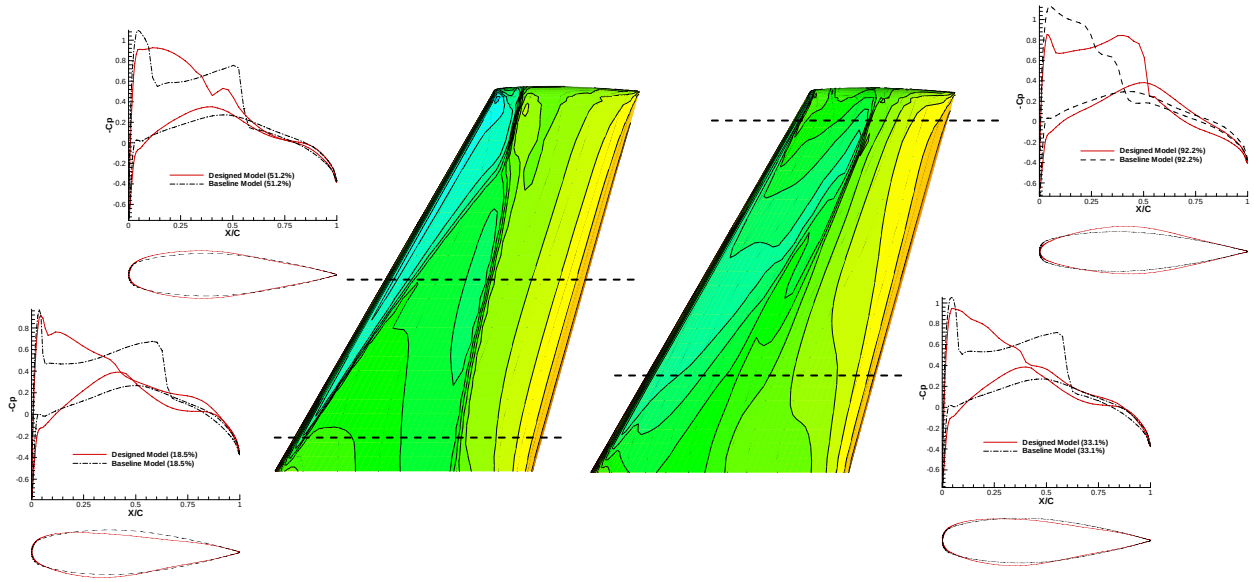

(a) Baseline Model (b) Designed Model

Fig. 14. Comparison of Surface Pressure Distribution

In the next case, more complicated design problem of wing/body configuration with very complex overset mesh system will be presented to validate the capability of the overset design tools in more practical usage. More complicated design work using 7 blocks of overset mesh system over DLR-F4 wing/body configuration is performed. Totally 200 design variables on 10 design sections on wing surface are used. On each design section, 20 Hicks-Henne functions are used similarly to the transonic wing design problem. As mentioned before, there are three component blocks – collar block, wing block, and tipcap block - are overlapped on the wing surface. To deform the surface meshes during the design procedure, the overlapped meshes are mapped onto the planform. The deformation for the overlapped surface meshes which are coexist on the same coordinate in the planform is equally. The design history in Fig. 15 shows that the drag is changed from 0.0227 to 0.0202(12% reduction) through 10 design iterations. Considering the drag portion of fuselage, the quantity of its decrease is quite reasonable, because the quantity of drag decrease for wing only reaches about 17% as shown in table 1. The L/D is changed from 32.26 to 36.25(12.3% increase). It is observed in Fig. 16 that the shock strength on the designed wing surface is diminished considerably. From the observation of design problems for transonic aircraft geometries, the present design tools for overset mesh system can be generally applied to the design problems of complex aircraft geometries.

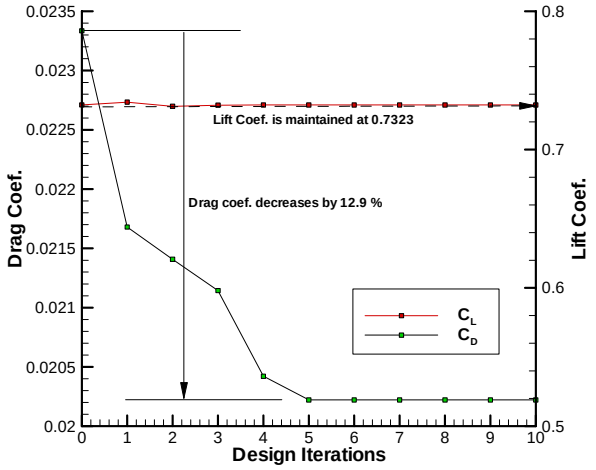

Fig. 15. Design History (DLR-F4)

	Baseline	Designed Model	Δ(%)
Fuselage	6.3270E-03	6.3263E-03	-1%
Wing	1.6384E-02	1.383E-02	-17%

Table. 1. Drag Distribution on the Component

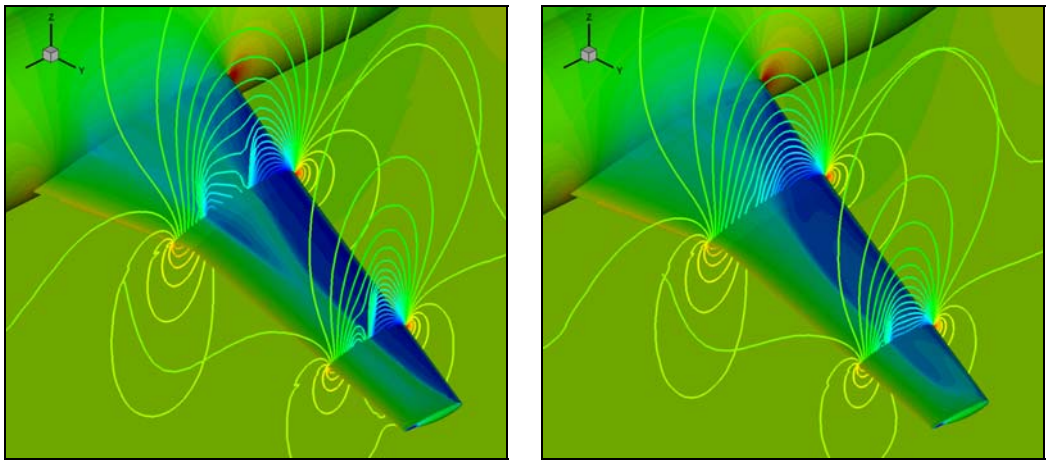

(a) Baseline Model (DLR-F4) (b) Designed Model

Fig. 16. Comparison of Flow Pattern between Baseline Model and Designed Model

6. Conclusions

A new optimal design approach based on overset mesh technique and adjoint formulas. Especially, the overset boundary conditions for discrete adjoint variable method are carefully derived. Overset flow analysis techniques are adequately adapted to the sensitivity analysis code and design modules by improvement or development. For the pre-processing of the overset flow analysis and sensitivity analysis, finding block connectivity is automatically carried out by overlap optimization. And improvement of convergence characteristics can be achieved in adjoint variable code through the overlap optimization. For the post-processing code, the aerodynamic coefficients are evaluated by Spline-Boundary Intersecting Grid Scheme (S-BIG) for convenient calculation of {dF/dQ} term in the sensitivity analysis. W.R.T. the grid modification in the design process, the overlapped surfaces of collar, wing, tipcap blocks can be displaced simultaneously by mapping from planform to wing surface. The present design approach with the special techniques for overset mesh system, successfully demonstrated its capability for the aerodynamic shape optimization of complex geometry design problems.

7. Acknowledgement

The authors appreciate financial support by the Brain Korea-21 Project for the Mechanical and Aerospace Engineering Research at Seoul National University and by the Korea Science and Engineering Foundation (Grant R01 -2005-000-10059-0)

8. References

1. William M. Chan, Reynaldo J. Gomez III, Stuart E. Rogers, Pieter G. Buning. Best Practices in Overset Grid Generation. AIAA Paper 2002-3191
2. C. L. Rumsey, Robert T. Biedron. Computation of Flow Over a Drag Prediction Workshop Wing/Body Transport Configuration using CFL3D. NASA TM-2001-211262
3. K. Leoviriyakit, S. Kim, and A. Jameson. Viscous Aerodynamic Shape Design Optimization of Wings including Planform Variables. AIAA Paper 2003-3498.
4. S. Choi, J.J. Alonso, S. Kim, I. Kroo, and M. Wintzer. Two-Level Multi-Fidelity Design Optimization Studies for Supersonic Jets. AIAA Paper 2005-0531.
5. B.J. Lee, C. Kim, and O. Rho. Optimal Shape Design of the S-Shaped Subsonic Intake Using NURBS. AIAA Paper 2005-0455.
6. E.J. Nielsen, and W.K. Anderson. Aerodynamic Design Optimization on Unstructured Meshes Using the Navier-Stokes Equations. AIAA Paper 98-4809.
7. H.J. Kim, D. Sasaki, S. Obayashi, and K. Nakahashi. Aerodynamic Optimization of Supersonic Transport Wing Using Unstructured Adjoint Method. AIAA Journal, 2001, 39(6): 1011-1020.
8. S. Nadarajah, A. Jameson. Studies of the Continuous and Discrete Adjoint Approaches to Viscous Automatic Aerodynamic Shape Optimization. AIAA Paper 2001-2530.
9. C.S. Kim, Chongam Kim, O.H. Rho. Feasibility Study of Constant Eddy-Viscosity Assumption in Gradient-Based Design Optimization. Journal of Aircraft, 2003, 40(6):1168-1176.
10. W. Liao, and H.M. Tsai. Aerodynamic Design Optimization by the Adjoint Equation Method on Overset Grids. AIAA Paper 2006-54.

11. Ralph W. Noack, and Davy M. Belk. Improved Interpolation for Viscous Overset Grids. AIAA Paper 97-0199.
12. Norman E. Suhs, Stuert E. Rogers, and William E. Dietz. PEGASUS 5: An Automated Pre-processor for Overset-Grid CFD. AIAA Paper 2002-3186.
13. J. C. Vassberg, P. G. Buning, and C. L. Rumsey. Drag Prediction for the DLR-F4 Wing /Body using OVERFLOW and CFL3D on an Overset Mesh. AIAA Paper 2002-0840.
14. R.L. Meakin. Object X-rays for Cutting Holes in Composite Overset Structured Grids. AIAA Paper 2001-2537.
15. D.M. Belk, and R.C. Maple, "Automated Assembly of Structured Grids for Moving Body Problems," AIAA Paper 95-1680.
16. D.L. Brown, W.D. Henshaw, and D.J. Quinlan. Overture: Object-Oriented Tools for Overset Grid Applications. AIAA Paper 99-3130.
17. W.M. Chan and P.G. Buning. Zipper Grids for Force and Moment Computation on Overset Grids. AIAA Paper 95-1681.
18. Nathan Hariharan, Z.J. Wang, and P.G. Buning. Application of Conservative Chimera Methodology in Finite Difference Settings. AIAA Paper 97-0627.
19. Sung-soo Kim, Chongam Kim, Oh-hyun Rho, and Seung Kyu Hong. Cures for the Shock Instability: Development of Shock-Stable Roe Scheme. Journal of Computational Physics, 2003, 185(2): 342-374.
20. J.R.R.A.Martins, I.M.Kroo, and J.J.Alonso. An Automated Method for Sensitivity Analysis using Complex Variables, AIAA Paper 2000-0869.